

Introducing HYDRA

A Multispectral Data Analysis Toolkit

BY TOM RINK, W. PAUL MENZEL, PAOLO ANTONELLI, TOM WHITTAKER,
KEVIN BAGGETT, LIAM GUMLEY, AND ALLEN HUANG

DESIGN PHILOSOPHY OF HYDRA. HYDRA (Hyper-spectral Data Viewer for Development of Research Applications) grew out of the necessity to provide research scientists and educators with freely available software that could display and analyze remotely sensed multispectral and hyperspectral data. HYDRA is a third-generation application for hyperspectral data produced at the University of Wisconsin's Space Science and Engineering Center (SSEC) and Cooperative Institute for Meteorological Satellite Studies (CIMSS). The first two were based on commercial packages IDL and Matlab and served as a test bed to refine the operations and functionality required by the users.

When considering the design of HYDRA, the most important requirements were that the software must be a) freely available to the global community, b) computer platform independent, and c) extendable. Computer platform independence has been elusive in so far as hierarchical data format (HDF) libraries are still required to view the data. It was also important that the tool kit be coded in an easy-to-use scripting language, so that users could modify and extend the capabilities as needed. The Visualization for Algorithm Development (VisAD) Java library was selected as the basis for HYDRA. This library allows applications to be written in either Java or Jython, the Java implementation of the popular Python scripting language. The core of the VisAD library is a unified Data Model, which allows for the representation of literally any numeric

data in a consistent manner. This is very important when integrating data from a variety of sources that may have different sampling topologies in space or time. The data model also has built-in metadata for parameters such as units and error estimates. Because these metadata are an integral part of the data means they can be easily used to verify the validity of computations (the software detects invalid combinations, such as adding a temperature to a pressure) and to estimate the reliability of computations.

HYDRA has been developed using the Jython scripting language. The syntax of this language is simple enough that it lends itself to easy modifications by end users who are either more familiar with scripting languages or are already competent Java programmers. Like other scripting languages, Jython suffers from poor computing performance; however, this is not an issue with HYDRA, as nearly all "heavy" computing is handled by the VisAD library.

The programmatic interface to the data files has been designed so that emerging new file types or formats will be easy to support without changing the core of the applications. The key was to keep the reading of the files abstract so that the application makes the same function or method calls regardless of the file being read. This same philosophy is used in packages such as OpenDAP and ESML, which have the notion of a plug-in.

The online supplement for this article offers more details on getting HYDRA started and how to use the command structure to stage and interrogate multispectral data. The following sections illustrate some of the capabilities for analyzing multispectral Moderate Resolution Imaging Spectroradiometer (MODIS) and hyperspectral Atmospheric Infrared Sounder (AIRS) data with HYDRA. HYDRA is also capable of viewing and interrogating data from the Geostationary Operational Environmental Satellite (GOES) imager data as well as the European Meteosat Spinning Environmental Visible and InfraRed Instrument (SEVIRI).

AFFILIATIONS: RINK, ANTONELLI, WHITTAKER, BAGGETT, GUMLEY, AND HUANG—Cooperative Institute for Meteorological Satellite Studies, Madison, Wisconsin; MENZEL—NOAA Satellite and Information Services/ORA, Madison, Wisconsin

CORRESPONDING AUTHOR: W. Paul Menzel, NOAA/NESDIS, 1225 W. Dayton Street, Madison, WI 53706
E-mail: Paul.Menzel@noaa.gov

DOI:10.1175/BAMS-88-2-159

©2007 American Meteorological Society

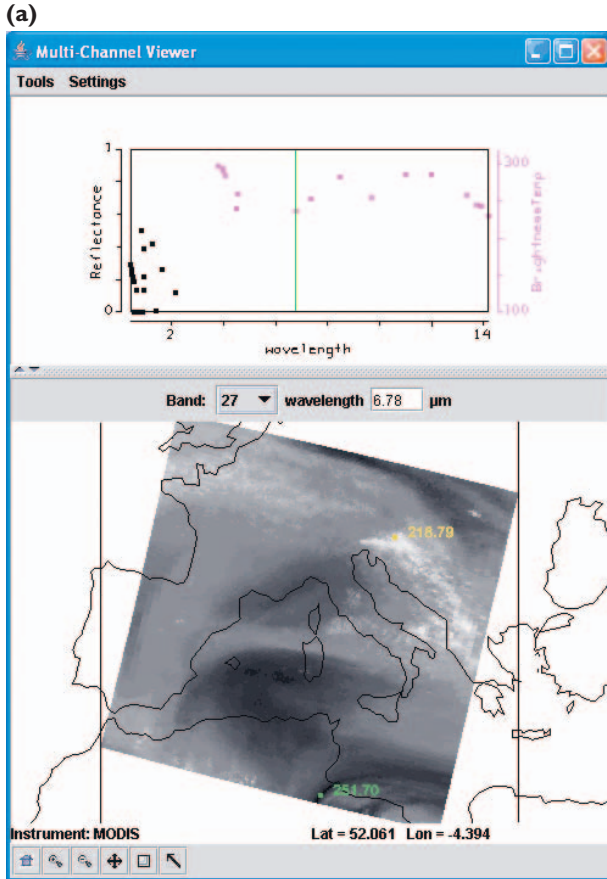
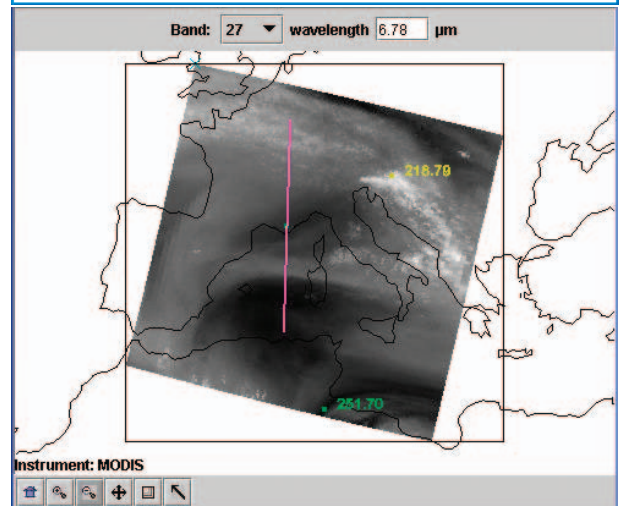
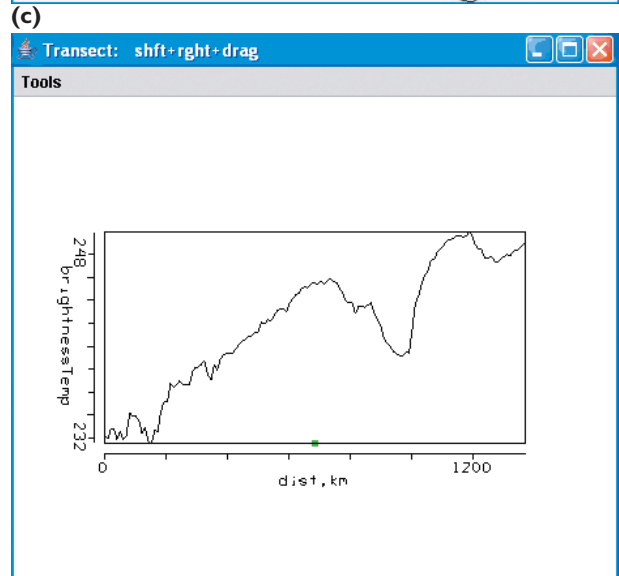
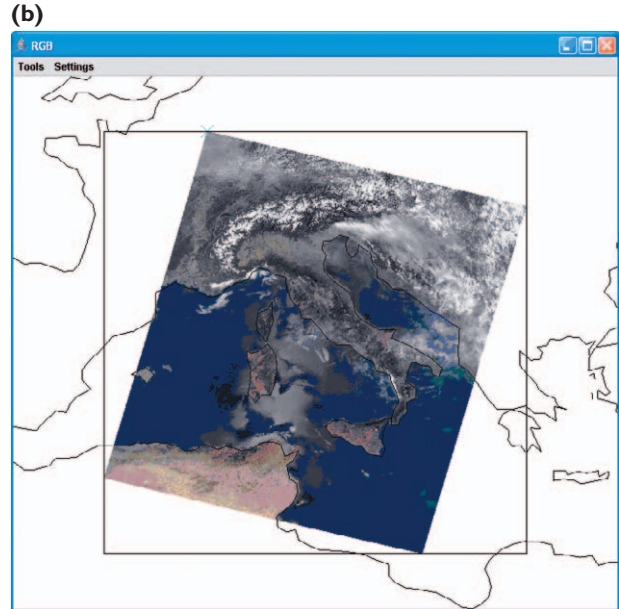


FIG. 1. (a) “Multi-Channel Viewer” of a MODIS granule from 29 May 2001 over Europe at 1030 UTC. The upper panel shows the 36-channel spectrum of the reflectance measurements in the visible and near-infrared channels (black dots referenced to the left y-axis) and the brightness temperature measurements in the infrared channels (purple dots referenced to the right y-axis) as a function of wavelength (microns). The lower panel shows the water vapor image with minimum (219 K) and maximum (252 K) superimposed.

(b) A pseudo-RGB image composed in the multi-channel viewer using the RGB option under “Tools.” The red channel is using channel 1 ($0.65 \mu\text{m}$), the green channel is using channel 4 ($0.56 \mu\text{m}$), and the blue channel is using channel 3 ($0.47 \mu\text{m}$). The reflected solar contributions in the Mediterranean Sea are clearly visible.

(c) Water vapor brightness temperatures (top) for a transect in the $6.78\text{-}\mu\text{m}$ water vapor brightness temperature image (bottom) starting at clouds in northern Europe and progressing through the Alps and then through two dry regions west of Italy. The two dry regions are more than 10 K warmer than the moister region.



EXAMPLES OF MULTI-CHANNEL VIEWING WITH HYDRA.

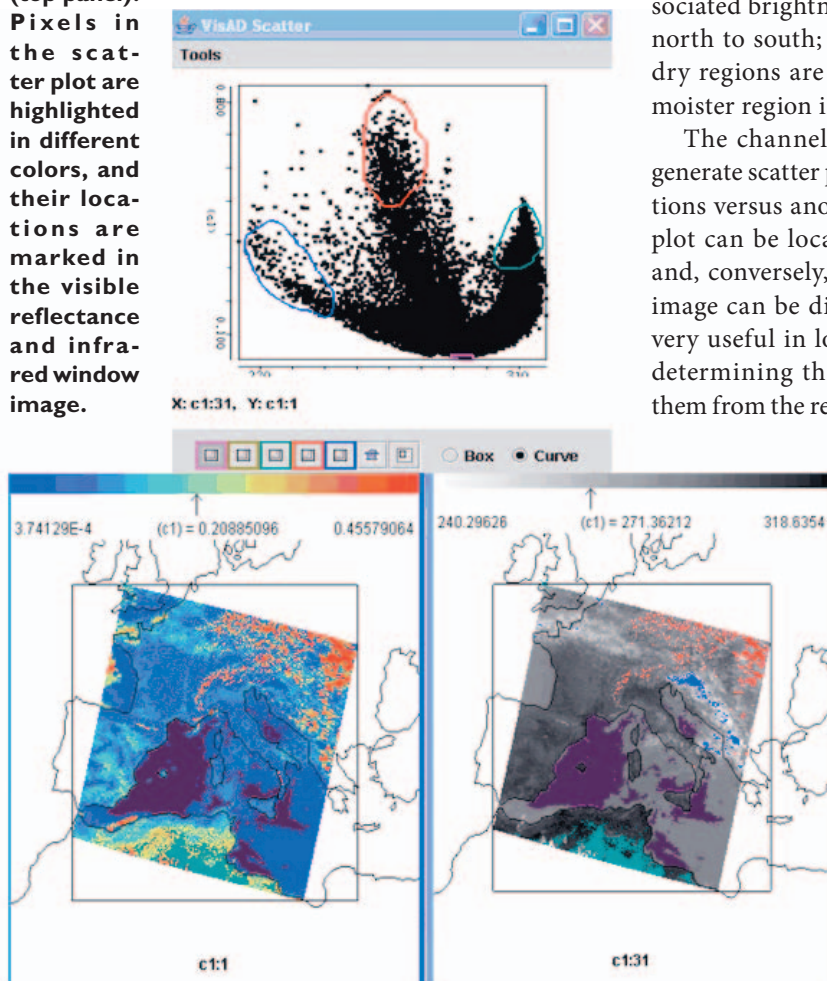
The multi-channel viewer enables display and interrogation of the 36 spectral channel values for any pixel within a granule of MODIS data [consisting of 335.3 megabytes(MB)]. Measurement values (in radiance and reflectance or brightness temperature as selected) can be displayed for individual pixels within the granule; transects from one location to another can be constructed for a given spectral channel to determine min/max values as well as gradients in between. Figure 1a shows the water vapor channel ($6.78 \mu\text{m}$) brightness

temperature image from a granule of MODIS data for 1030 UTC on 29 May 2001 over Europe (dark is warm and white is cold) below a plot of the reflectances (for the visible and near-infrared channels) and the brightness temperatures (for the infrared channels) associated with the warmest and coldest pixels in the granule. Using the HYDRA commands, measurement values and latitude/longitudes for any of the pixels (for all of the spectral channels) can be displayed. Figure 1b demonstrates the RGB option where a false-color image can be composed in the “Multi-Channel Viewer” using the RGB option under “Tools.” This MODIS channel combination (channel 1 at $0.65 \mu\text{m}$ in the red, channel 4 at $0.56 \mu\text{m}$ in the green, and channel 3 at $0.47 \mu\text{m}$ in the blue) comes closest to providing an image akin to what the human eye would see; note the reflected solar contributions over the Mediterranean Sea. RGB allows any three channels to drive the red, green, and blue enhancements. Figure 1c shows a transect superimposed on the water vapor image and the associated brightness temperature values going from north to south; it is readily apparent that the two dry regions are more than 10 K warmer than the moister region in between.

The channel combinations tool allows one to generate scatter plots of one set of channel combinations versus another. The values within the scatter plot can be located in the multi-channel images, and, conversely, regions within the multi-channel image can be displayed in the scatter plot. This is very useful in locating features in the images and determining threshold values for discriminating them from the rest of the image (e.g., clear sky versus cirrus clouds).

Figure 2 shows screens enabled by the channel combinations tool. Visible reflectances (left) are plotted against infrared window $11\text{-}\mu\text{m}$ brightness temperatures (right) on the y -axis and x -axis, respectively, in a scatter plot (center). Pixels in the scatter plot are highlighted in different colors and their locations are marked in the visible reflectance and infrared window brightness temperature images. Coldest temperatures and low reflectances indicate clouds (blue), highest reflectances and freezing temperatures indicate snow in the

FIG. 2. Screens enabled by the channel combinations tool. Visible reflectances (color enhanced in the bottom left panel with near-zero reflectance blue, 20% reflectance green, and 50% reflectance red) are plotted against infrared window $11\text{-}\mu\text{m}$ brightness temperatures (in the bottom right panel where cold temperatures of 240 K are white and hot temperatures of 319 K are black) on the y -axis and x -axis, respectively, in a scatter plot (top panel).



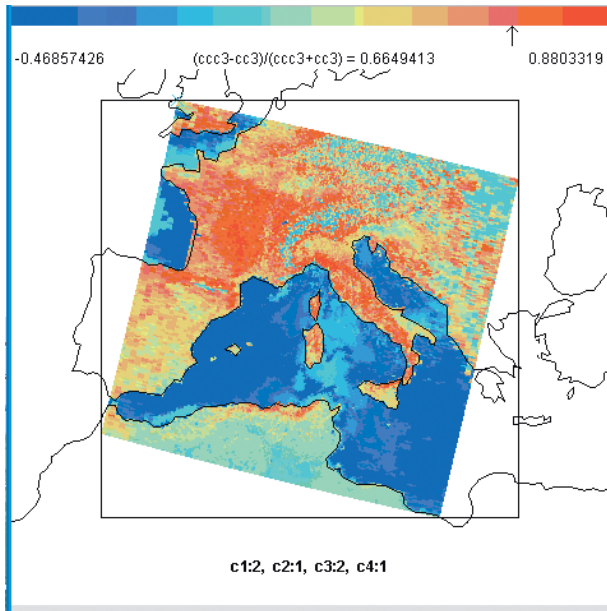


FIG. 3. A pseudo-image of normalized vegetation index constructed with MODIS reflective bands [band 2 (0.86 μm) – band 1 (0.65 μm)] / [band 2 (0.86 μm) + band 1 (0.65 μm)]. Dry desert-like areas in the northern regions of Africa show vegetation indices below 0.2 (turquoise); fertile river valleys and coastal regions show indices above 0.6 (red). Ocean areas show negative values (blue). The arrow indicates the median value in the scene.

Alps and elsewhere (red), near-zero reflectances and temperatures around 290 K indicate nearshore waters (purple), and hottest temperatures and modest reflectances indicate desert (turquoise). Conversely, pixels in the images can also be highlighted and their locations in the scatter plot marked (not shown).

Figure 3 shows an example of an image created from linear combinations of spectral channels with HYDRA; the normalized vegetation index is shown as calculated from reflectances [band 2 (0.86 μm) – band 1 (0.65 μm)] / [band 2 (0.86 μm) + band 1 (0.65 μm)]. The vegetation index is based on the relatively low leaf and grass reflectance from spectral bands below 0.72 μm and relatively high reflectance from spectral bands above. Regions with some vegetation are clearly distinguished from those with little. Regions without significant vegetation have indices below 0.3; vegetated regions show indices above 0.6.

HYPERSPECTRAL DATA ANALYSIS WITH HYDRA. HYDRA is also used to analyze granules of hyperspectral AIRS data (consisting of about 63 MB each); the spectral selection is now

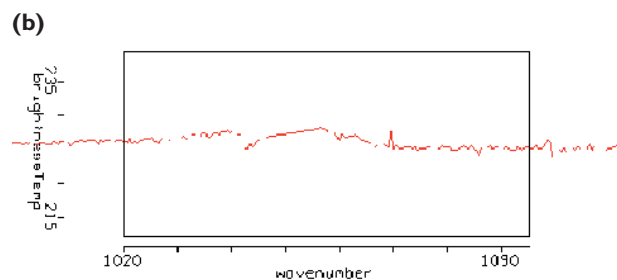
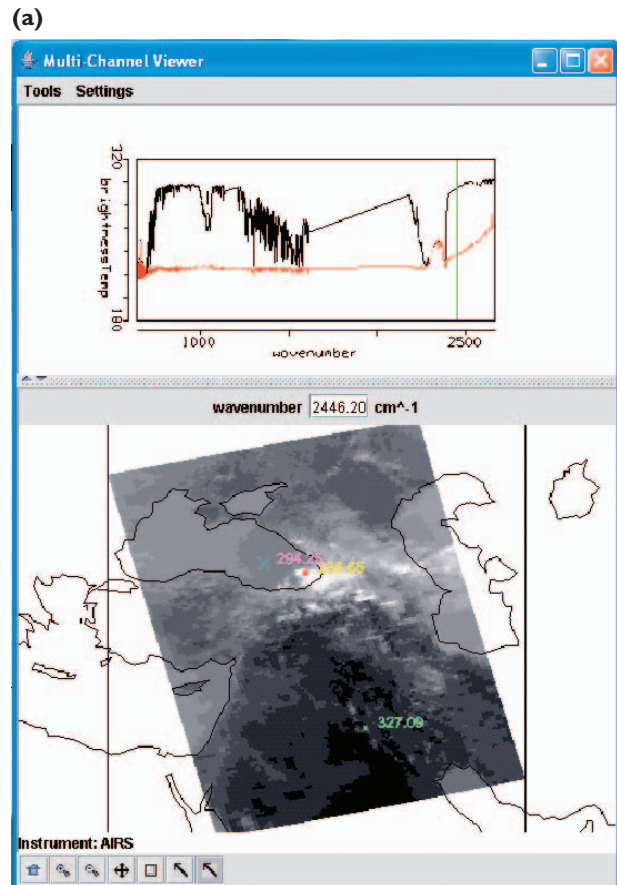


FIG. 4. (a) Multi-channel viewer display of AIRS data over the Black and Caspian Seas on 28 Aug 2005 showing spectra (top) and short wave (2446 cm^{-1}) infrared window image (bottom). Brightness temperature spectra from 650 to 2550 cm^{-1} are measured by AIRS over the pixel in the Black Sea (marked by the “x”) and over the nearby pixel in the high clouds (marked by the red dot). Straight lines in the spectra cover the spectral gaps in the AIRS measurements. Black Sea brightness temperatures in the infrared window regions are near 300 K, while the cloud-top temperatures are about 220 K. (b) Zoom of the ozone absorption region near 1050 cm^{-1} in the spectra observed over the cloudy pixel (marked by the red dot in Fig. 4a). Cloud temperatures get warmer by about 3 K in the spectral region that is more opaque to ozone, indicating that the cloud top is likely in the stratosphere.

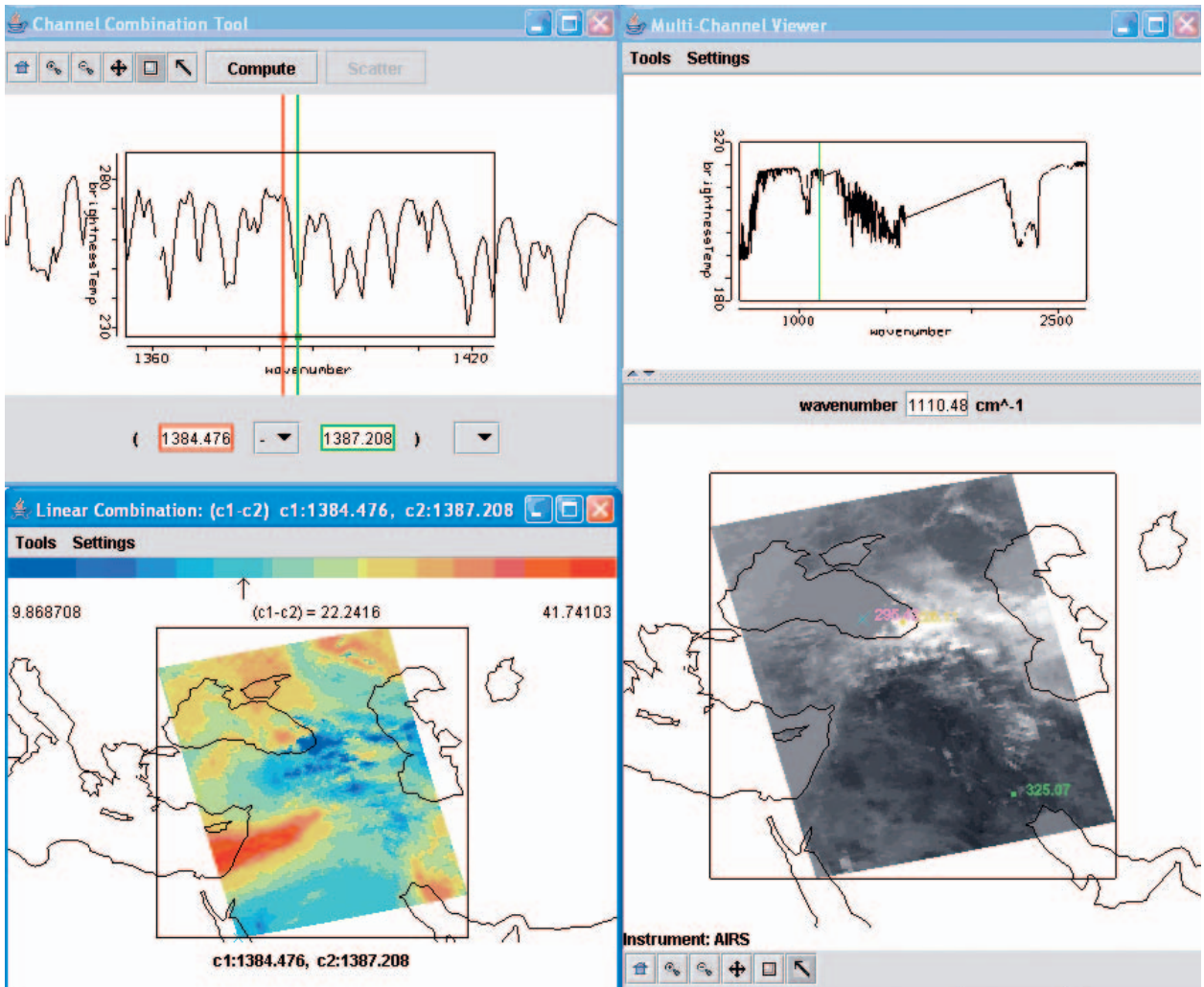


FIG. 5. (Right) AIRS-measured spectrum in western part of the Black Sea (marked by the “x”) and the infrared window image from 1110.5 cm^{-1} . (Top left) Channel combinations display of brightness temperature spectrum between 1420 and 1360 cm^{-1} in the water vapor absorption spectral region. (Bottom left) Brightness temperature differences of 1384.5 cm^{-1} (off the water vapor rotational absorption line) minus 1387.2 cm^{-1} (on the water vapor rotational absorption line). Brightness temperature differences of more than 40 K are seen in clear regions and less than 1 K in opaque high cloudy regions, indicating the spectral and spatial sensitivity of the AIRS measurements.

indicated by wavenumber, a prevalent indicator in the infrared region of the spectrum which equals the number of wavelengths that fit into 1 cm. AIRS takes infrared measurements from 650 to 2550 cm^{-1} (15.4 to 3.9 μm) in 2300 spectral bands at spectral resolutions as high as 0.5 cm^{-1} . Figure 4a shows the multi-channel viewer display of AIRS data over the Black and Caspian Seas on 28 August 2005. The top panel displays two spectra measured by AIRS over a pixel in clear skies in the Black Sea (marked by the “x” and displayed as the black spectra) and over a nearby pixel in high clouds (marked by the red dot and displayed by the red spectra); the spectral gaps

in AIRS between 1136 and 1265 cm^{-1} (8.8 and 8.2 μm) and 1629 and 2169 cm^{-1} (6.2 and 4.6 μm) are bridged by HYDRA with a straight line. The clear-sky spectrum shows those regions where the atmosphere has CO_2 absorption (between 650 and 750 cm^{-1} as well as between 2350 and 2450 cm^{-1}), H_2O absorption (between 1265 and 1625 cm^{-1}), and O_3 absorption (near 1050 cm^{-1}). Black Sea brightness temperatures in the infrared window regions are near 300 K, while the cloud-top temperatures are about 220 K. The spectral brightness temperatures measured over the cloud are relatively constant, as one would expect over an opaque blackbody-like

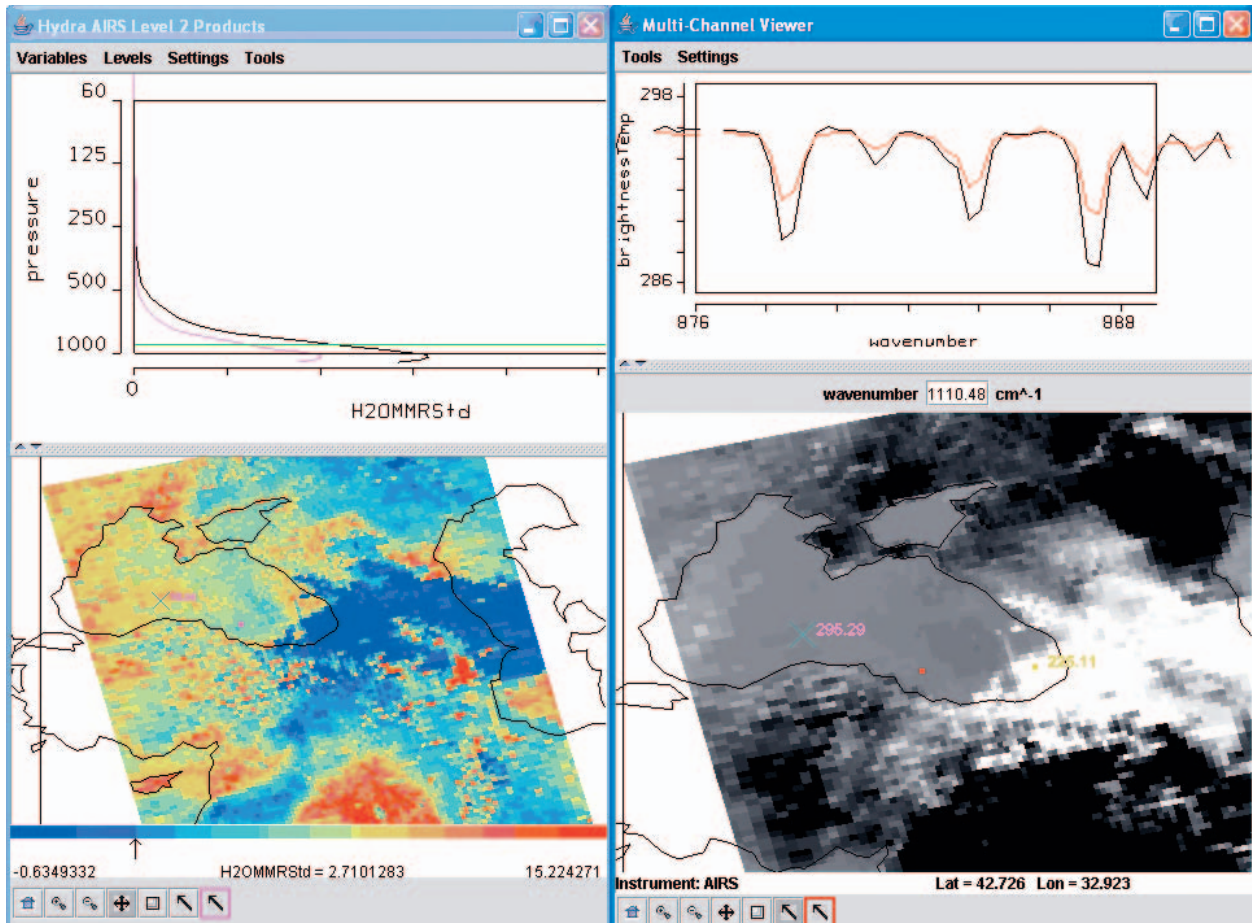


FIG. 6. (Top right) AIRS measured spectra from 876 to 888 cm^{-1} in western (marked by the “x”) and eastern (marked by red dot) locations in the Black Sea in the infrared window image from 1110.5 cm^{-1} . The online-offline brightness temperature difference is greater in western locations of the Black Sea. (Bottom right) AIRS 1110.5 cm^{-1} brightness temperature image indicating the two locations in the Black Sea for the measured spectra shown top right. (Top left) Water vapor profiles (in mm) associated with the western (black profile) and eastern (purple profile) locations in the Black Sea. The western location is substantially moister. (Bottom left) Image of water vapor retrieval field at 900 hPa for the AIRS granule showing the gradients more clearly (with blue indicating little or no 900-hPa moisture, and red indicating 15 mm).

cloud in the long wavelength region (the spectra is relatively flat between 650 and 1150 cm^{-1}). No significant moisture is evident above the cloud (indicated by the flatness in the water vapor-sensitive region between 1265 and 1625 cm^{-1}). In contrast, there is strong absorption by atmospheric water vapor over the surface of the Black Sea (resulting in significantly colder brightness temperatures from 1300 to 1600 cm^{-1} , since the sensor is seeing less deeply into the troposphere) and absorption by atmospheric ozone (seen in the colder temperatures near 1050 cm^{-1}). The reflected solar contribution over the cloud in the short wavelength region is evident by the temperature increase from 220 to

260 K (going from 2450 to 2550 cm^{-1}). However, there is no significant solar contribution from the Black Sea pixel.

Figure 4b demonstrates the capability to zoom in on a portion of the spectra. As one nears the center of the ozone absorption region, it is expected that the satellite is sensing less deeply into the atmosphere. As the cloud temperatures get warmer by about 3 K in going from the periphery of the ozone absorption band at 1020 cm^{-1} to the center of the absorption band at 1055 cm^{-1} , it is suspected that the cloud top is likely in the stratosphere where temperatures get warmer with altitude (unlike the troposphere, where they get colder with altitude).

Figure 5 shows the channel combinations tool enabling investigation of spectral channels on and off water vapor absorptions features; this illustrates how the spectral and spatial sensitivity of the AIRS measurements is readily explored with HYDRA. Brightness temperature differences of 1384.5 cm^{-1} (off the water vapor rotational absorption line) minus 1387.2 cm^{-1} (on the water vapor rotational absorption line, hence sensing more of the lower tropospheric moisture) of more than 40 K (red regions in lower left image) indicate very moist regions of the lower troposphere; dry regions (blue) with less than 1 K difference are evident over the desert and in opaque high clouds.

HYDRA also enables comparison soundings of temperature and moisture (generated from non-HYDRA software and staged into a file that HYDRA can read) with spectra from selected pixels. Figure 6 shows an example; moisture profiles and spectra in

the eastern and western parts of the Black Sea demonstrate that deeper water vapor absorption lines are associated with moister atmospheres. The profile retrievals have been accomplished with a principal component retrieval algorithm trained with AIRS spectra calculated from radiosonde observations.

HYDRA also offers the capability to collocate MODIS and AIRS data gathered from *Aqua*. The MODIS and AIRS granules are opened separately with the HYDRA, and the position arrows automatically start tracking in each display. Figure 7 shows an example where collocated MODIS data is suggesting subpixel cloud presence in the AIRS data.

SUMMARY. As these few examples illustrate, HYDRA offers several tools to interrogate multispectral and hyperspectral remote-sensing data quantitatively and to explore the correlations between radiance measurements and features in the images. Continued

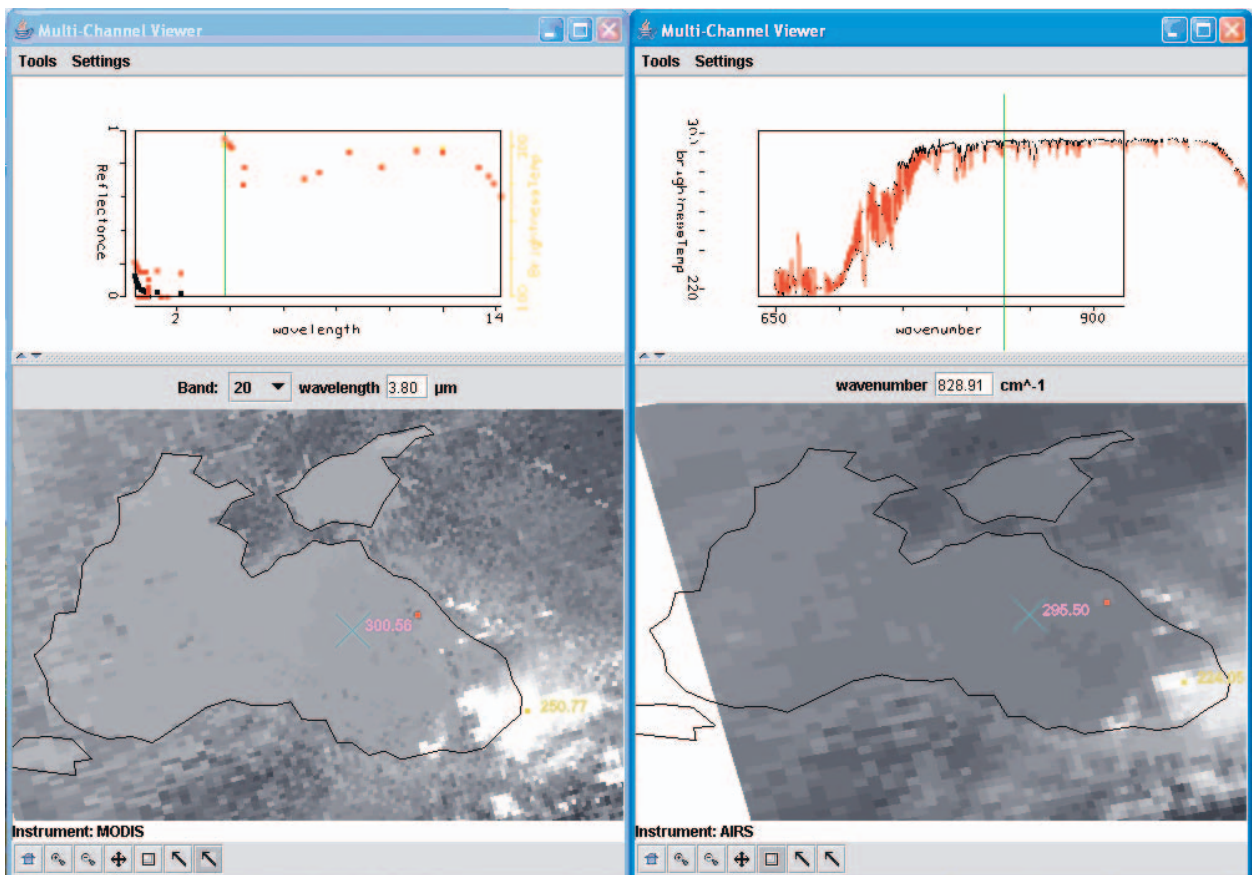


FIG. 7. HYDRA with AIRS (right) and MODIS (left) collocated display of spectra. The MODIS 3.8- μm image is indicating some cloud contamination in the location of the red dot; the cloudy spectra (red) is cooler than the clear-sky spectra in the location of the “x” (yellow). The AIRS 828 cm^{-1} ($\sim 12\text{ }\mu\text{m}$) image does not reveal the cloudiness, but the clear-sky spectra (black) is slightly warmer than the suspected cloudy spectra (red).

development over the next several years is planned in order to incorporate more multispectral and hyperspectral instrument systems into the HYDRA menu. In addition, several improvements will be added, including 1) improving the user interface; 2) adding the capability to animate sequences in time or wave-number; 3) introducing a state-saving device (i.e., a persistence mechanism); 4) enhancing collaboration at remote sites through granule sharing; 5) enabling more high-spectral data analysis (i.e., principal component analyses); and 6) providing more interaction between scripting and the application.

The World Meteorological Organization (WMO) has added HYDRA to its Virtual Laboratory for Satellite Training and Data Utilization to enable research with satellite data and to enhance training capabilities. The Virtual Laboratory is designed to provide the instructors and students with a set of easy-to-use tools for creating and conducting training sessions—HYDRA is now part of this international tool kit.

The HYDRA project is an ongoing development effort. Planned future developments include features that will enable remote multiple-site viewing of and interaction with the same dataset; this will enhance use in the Virtual Laboratory and collaborations at remote sites.

More information and the freeware may be found at: www.ssec.wisc.edu/hydra.

ACKNOWLEDGMENTS. This paper relied on the active participation in beta testing of the HYDRA freeware

by many students and international colleagues. We thank them for their enthusiasm and useful feedback.

FOR FURTHER READING

- Aumann, H. H., and Coauthors, 2003: AIRS/AMSU/HSB on the Aqua Mission: Design, science objectives, data products, and processing systems. *IEEE Trans. Geosci. Remote Sens.*, **41**, 253–264.
- Barnes, W. L., T. S. Pagano, and V. V. Salomonson, 1998: Prelaunch characteristics of MODIS on EOS-AM1. *IEEE Trans. Geosci. Remote Sens.*, **36**, 1088–1100.
- Bill, R. W., 2002: *Jython for Java Programmers*. New Riders Publishing, 465 pp.
- Hibbard, W., and Coauthors, 2002: Java distributed objects for numerical visualization in VisAD. *Comm. ACM*, **45**, 160–170.
- King, M. D., Y. J. Kaufman, W. P. Menzel, and D. Tanre, 1992: Remote sensing of cloud, aerosol and water vapor properties from the Moderate Resolution Imaging Spectrometer (MODIS). *IEEE Trans. Geosci. Remote Sens.*, **30**, 2–27.
- Lutz, M., 1996: *Programming Python*. O'Reilly & Associates, 880 pp.
- Weisz, E., H.-L. Huang, J. Li, S. Seemann, E. Borbas, and L. Gumley, 2005: AIRS real-time sounding profile retrieval for IMAPP (International MODIS/AIRS Processing Package) Users. *Tech. Proc. 13th International TOVS Study Conf.*, St. Adele, Canada, 323–330.